Hindawi
Advances in Materials Science and Engineering
Volume 2022, Article ID 2388622, 13 pages
https://doi.org/10.1155/2022/2388622

Research Article

Device for Simulating Fluid Microgravity Environment Based on Magnetic Compensation Method and Research on Magnetic Fluid Lubrication Performance of Oil Film Bearing

Han Peng, Linjian Shangguan, and Hai Zhang

School of Mechanical Engineering, North China University of Water Resource and Electric Power, Zhengzhou 450045, Henan, China

Correspondence should be addressed to Linjian Shangguan; shangguanlinjian@ncwu.edu.cn

Received 16 September 2021; Revised 2 December 2021; Accepted 3 January 2022; Published 18 January 2022

Academic Editor: Wei Liu

At present, with the rapid development of the material market, the requirements of high performance and high precision of materials are increasingly exposed. Nanomagnetic fluid materials are more and more widely used in oil film bearings, but their compressive strength and performance are insufficient, which is difficult to meet the current requirements of material chemical properties. First of all, a device for simulating a microgravity environment with magnetic compensation is fabricated. Then, in the microgravity environment, according to the different proportions of magnetic solid particles, the base carrier liquid and the surfactant are mixed to produce nanomagnetic fluid and the nanomagnetic fluid with different composition proportions is prepared by adjusting the proportion of ferrous and ferric ions. Finally, the lubrication performance of oil film-bearing magnetic fluid with different composition ratios was tested. The results show that when the ratio of Fe^{2+} to Fe^{3+} is between 11 : 20 and 13 : 20, the MHD (magnetohydrodynamics) lubrication performance of oil film bearing is in the peak region. When the ratio is 3 : 5, the best lubrication performance can be achieved. When it is slightly higher than this ratio, the oxidation rate is accelerated due to more ferrous ions. Although it can have a good lubrication effect, it is easy to cause the overall fluidity of oil film-bearing magnetic fluid to deteriorate. Therefore, the oil film bearing nano-MHD with the ratio of 3 : 5 ferrous to ferric has the best lubrication performance in the microgravity environment simulated by magnetic compensation. Experiments have shown that when the magnetic fluid is heated in a magnetic field, the temperature gradient will cause the magnetization to change, which makes the magnetic force experienced by the liquid in each part different, causing convection. Therefore, by selecting the direction of the magnetic field and the heating surface, by applying an external magnetic field or promoting convection, or suppressing convection, convection in the opposite direction to the natural convection of gravity can also be realized. Moreover, magnetism can immediately promote high-temperature boiling, generate bubbles, and eliminate the generation of bubbles to promote heat transfer. With the above effects, the heat conduction between the heating wall and the liquid can be controlled, and its practical and potential application fields are very wide.

1. Introduction

In recent years, magnetic fluid lubrication technology has developed rapidly at home and abroad because of its many advantages. According to the characteristics of the relatively uniform magnetic field distribution of the Helmholtz coil, a suitable alternating magnetic field generator is designed. When the load is large, the pressure on the bearing surface makes the bearing produce elastic deformation. On the other hand, the temperature rise will also cause large thermal deformation of the bearing. The deformation of the bearing will cause the change of oil film distribution, which will affect the lubrication performance. Therefore, under the condition of heavy load, it is necessary to consider the influence of bearing deformation on lubrication performance.

In the research of MHD coil, Kakutani analyzed the MHD lubricated coil in detail and gave the coil design parameters suitable for different parts of the tumor lubrication through

simulation [1]. Romig has developed the first lubrication prototype in China, which has been applied to magnetic field research after several iterations [2]. The research and preparation of magnetic fluid are also developing rapidly. Ziemer and Bush made a horizontal comparison of magnetic medium parameters and proposed optimization methods for different magnetic medium parameters [3]. Smith et al. summarized more than 30 studies on magnetic nanoparticles in the past five years and believed that the field is trying to minimize the side effects of lubrication on healthy cells [4]. Murakami and Okuno heat the tubular metal implants in the magnetic fluid through the magnetic fluid, but only when the magnetic fluid tissue of the lesion is relatively regular [5]. Su et al. confirmed that the warm moistening method above 42°C had an obvious killing effect on human MHD cells (QBC939). They also perfused hot saline into canine MHD by placing a catheter, but the temperature control was not accurate enough and the puncture was difficult [6]. Zhao et al. established the FMBD model of axial piston pump through AMESim and virtual platform, considering the influence of bearing and fluid vibration, and studied the noise transmission mechanism of axial piston pump combined with the test bench [7].

On bearing lubrication, Ahmad et al. conducted a theoretical study on the influence of the exciting force caused by the oil pressure in the plunger cavity on the vibration of the axial piston pump and built a test bench to verify the correctness of the theory [8]. Gülhan et al. simplified the structure of the axial piston pump, especially built a test bench for studying the oil film characteristics of the slipper pair, and measured the oil film thickness under different speeds and pressures under actual working conditions [9]. Based on the three-dimensional fractal theory, Smith et al. analyzed the nonlubricated contact of the rough surface and established the normal contact lubrication degree model of the fixed mechanical joint surface, and based on this model, the normal contact lubrication degree of the fixed mechanical joint surface under light load can be well predicted [10]. The above researches are mostly based on the elastohydrodynamic lubrication model, that is, the solid contact only has elastic deformation, and the lubrication is hydrodynamic lubrication, which often ignores the elasticity and elastoplasticity of the microconvex body when the actual contact pair bears medium and heavy load. The method in the overview only considers the elastic deformation of the object and does not consider its own bearing capacity in the actual process, which is one-sided.

This paper studies the device of magnetic compensation method to simulate fluid microgravity environment and the magnetic fluid lubrication performance of oil film bearing. First of all, a device for simulating a microgravity environment with magnetic compensation is fabricated. Then, in the microgravity environment, according to the different proportions of magnetic solid particles, the base carrier liquid and the surfactant are mixed to produce nanomagnetic fluid, and the nanomagnetic fluid with different composition proportions is prepared by adjusting the proportion of ferrous and ferric ions. Finally, the lubrication performance of oil film-bearing magnetic fluid with different composition ratios was tested.

2. Contact Lubrication and Amplitude Conversion of Nano-MHD

2.1. Dynamic Contact and Surface Activity Adjustment Method of Nanomagnetic Fluid. The fluid oil film is a kind of material that is sandwiched between two opposite sliding surfaces and has lubrication performance to achieve an antiwear effect. For the axial piston pump, the oil film characteristics between slippers are directly related to the overall performance and reliability life of the pump [11]. An axial plunger pump is a plunger pump in which the reciprocating direction of the piston or plunger is parallel to the central axis of the cylinder. An axial piston pump is a swashplate type axial piston pump that uses an oil distribution plate to distribute oil, the cylinder body rotates, and the variable head is variable. The pump adopts the optimal oil film thickness design of hydrostatic balance, so that the cylinder block and the oil distribution plate, the sliding shoe, and the variable head are operated under pure liquid friction. It has a simple structure, small volume, low noise, high efficiency, and long life. Longhe has the advantages of self-priming ability. The key parameter of oil film characteristics is viscosity, which directly affects the bearing capacity and leakage of oil film of slipper pair, and the most important factor of viscosity is temperature [12]. The purpose of this paper is to strengthen the pressure resistance of oil film bearings, expand the application range of oil film bearings, and meet the current social demand for materials. The temperature control system of the test bench can realize any variable temperature or constant temperature control required by the oil film test system of the slipper pair [13]. Therefore, temperature control is very important for the experimental study of fluid lubrication characteristics.

Under high preload, the average dynamic contact lubricity of nano-MHD increases with the increase of amplitude, but the overall value between the two kinds of interface is relatively similar. The main reason is that when the contact load increases, the actual contact area of the solid increases correspondingly, and the lubricant decreases [14, 15]. At this time, the dynamic contact lubricity of microconvex body plays a major role; therefore, it is approximate to the dynamic lubrication degree of the solid-solid nano-MHD interface [16, 17]. At the same time, it can be found that the theoretical model of solid-liquid interface is in good agreement with the experimental data, which verifies the correctness of the established model [18, 19]. The contact damping of the solid-liquid interface is much larger than that of the solid-consolidation interface, which is not of the same order of magnitude. With the increase of amplitude, the contact damping of the solid-liquid interface increases, while the increase of the solid-liquid interface is small [20]. In the low amplitude range, the solid-liquid interface data is smaller than the model, and in the high amplitude range, it is more consistent [21]. Due to the special location of the MHD tumor, it is necessary to strictly control the lubrication range and temperature to avoid irreversible damage to the surrounding normal MHD tissue. However, there are some defects in the above lubrication methods, such as fuzzy treatment area and nontreatment area, or high temperature, and easy to injure healthy tissue [22].

At low pressure, the slow development of the arc root will not only make the arc stagnate on the pantographed slide for a longer time but also cause the arc stretching speed to be slow due to the slow development and the arc length to maintain at a small level, and the arc is difficult to extinguish. The longer stagnation of arc root on the electrode under low pressure and the increase of arc duration due to the slow change of arc length make the arc corrode the pantograph catenary system electrode more seriously under low pressure [23]. At the same time, the temperature characteristics and shape characteristics of the arc under different gas pressures are analyzed. With the decrease of gas pressure, the overall temperature of the arc is slightly lower than that of the high gas pressure, but the decrease is not significant. It is worth noting that the diameter of the arc at lower air pressure is obviously larger than that at the higher air pressure, and the corresponding arc volume is also increased [24]. This is because, with the decrease of air pressure, the dynamic viscosity of the air decreases to a certain extent, which enhances the fluidity of the arc and increases the expansion degree of the arc column [25]. The increase of arc volume leads to the slow development of arc motion under the action of crosswind [26].

In addition, the stability of surfactants at high temperatures is poor, so a stable and efficient dispersant is needed to achieve the stable suspension of nanoparticles. Ionic liquids (ILs) have attracted researchers' attention because of their good stability at high temperatures, and they have good compatibility. It is reported that ionic liquids can also increase the critical micelle concentration of other additives in the base solution, so the mixed nanofluids with high-temperature stability can be obtained by compounding other surfactants with ionic liquids [27, 28]. From the point of view of the grinding process, although the cooling and lubrication conditions in the grinding zone can be improved to the maximum by adding nanoparticles, the penetration efficiency of grinding fluid is still difficult to be guaranteed due to the existence of the air barrier effect in the grinding process [29]. The internal cooling technology improves the structure of the tool so that the grinding fluid can directly wash the grinding area through the internal channel of the grinding wheel, which greatly improves the utilization rate of the grinding fluid, which is of great help to quickly reduce the temperature of the grinding area. The pressure term in the momentum equation and the product term of velocity and pressure in the energy equation are split, and then, a hybrid upwind scheme is constructed. In addition, the new convection pressure flux splitting method is that there is no pressure term in the convection flux. The mixed upwind scheme based on the convection pressure flux splitting method is simple in form and can capture contact discontinuities accurately. However, the "Ruby" phenomenon and postshock oscillation still appear in some problems. A new accurate and robust flux difference splitting scheme is constructed based on the Zha-Bilgen convection pressure flux splitting method. The pressure subsystem has a complete set of linearly independent eigenvectors, so the traditional flux difference splitting scheme can be constructed for calculation. The weak hyperbolic convection subsystem is calculated by the flux difference splitting scheme with the generalized eigenvector method. In order to improve the resolution of contact discontinuities, the BVD algorithm is used to reduce the density difference in the dissipation term of convective flux. Stability analysis and numerical experiments show that the new flux difference splitting scheme has better robustness and higher resolution than the roe scheme.

The surface morphology of the workpiece was obtained by traditional grinding fluid and mixed nanofluid. When the liquid supply pressure is low, deep processing lines appear on the surface of the workpiece, and the furrow is very obvious, which leads to local pits due to the phenomenon of material bonding. However, with the increase of liquid supply pressure in China's mechanical engineering, the surface of the workpiece is better improved, the furrow becomes shallower, smoother, and more regular, and the phenomenon of material bonding is reduced. This shows that increasing the supply pressure can effectively prevent the surface defects caused by the adhesion of wear debris, which is conducive to improving the processing performance. Compared with the surface morphology observed under different cooling and lubrication conditions at the same supply pressure, the surface morphology obtained by mixing nanofluids is more regular. The results show that the mixed nanofluids are helpful to improve the lubrication condition and surface quality of the grinding zone. When the feed pressure is 1 MPa, the profile fluctuation value of the two cooling media is 11.38 under the condition of traditional grinding fluid μ m. However, the profile fluctuation value decreases to 8.433 under the condition of mixed nanofluid grinding μ m. This is because the mechanism of grinding fluid in the grinding zone is boundary lubrication, and the lubrication effect mainly depends on the lubricating film. Compared with traditional grinding fluid, the mixed nanofluids are easier to form a lubricating film in the grinding zone, which avoids the direct contact between the abrasive particles and the workpiece. The existence of nanoparticles improves the bearing capacity of the lubricating film; under the physical synergism between ionic liquid and nanoparticles, the mixed nanofluids show excellent lubrication performance, which can effectively reduce the adhesion between grains and workpiece, and reduce the profile fluctuation of the machined surface. Therefore, better surface quality can be obtained by mixing nanofluids.

2.2. Algorithm for Normal Contact Lubrication and Amplitude Conversion of Nano-MHD. When the normal surface pressure is h and Y, respectively, and the excitation frequency is f, the experimental results of the solid-liquid interface are compared with the theoretical model:

$$H_i = F\left(\sum_{j=i}^{k} \omega_{ij} y_j - \theta_i\right) - C * Y, i \neq j,$$
$$Y_r = \left\| G_I - G_O \right\|_2. \tag{1}$$

Under low preload, the increasing trend of solid-liquid interface is relatively more obvious, and the dynamic contact lubrication degree of solid-liquid interface is greater than that of solid-solid interface s: under the same amplitude,

$$S_{ikjl} = \begin{cases} \dfrac{n}{\Delta_{ikjl}} \sqrt{\sum_{s=1}^{n} \left(x_{ik}(G) - x_{jl}(G)\right)^2 \Delta_{ikjl}(Y)} & \Delta_{ikjl} > 0; \\ 0 & \Delta_{ikjl} < 0 \end{cases}, \tag{2}$$

$$\frac{Y}{H} = \sum_{S-1}^{U} \sum_{d-1}^{K} f_s,\ DV_s,\ d.$$

By comparing the experimental data of solid-liquid interface with the theoretical simulation, it can be seen that there is a small jump in the experimental data, but the overall trend is consistent with the theoretical derivation:

$$R\left(D_i, w_j\right) = R\left(d_i\right)P\left(w_j|d_i\right); T\left(w_j|d_i\right) = \sum_{k=1}^{K} T\left(w_j|z_k\right)P\left(z_k|d_i\right),$$
$$T = \{P_1|D, L, f_2, Q, d, l \quad P_2|f_1, \mu\, P_3|N, M, I\}. \tag{3}$$

When the normal surface pressure is R and t, respectively, and the excitation amplitude is p, the dynamic contact lubrication degree changes with the excitation frequency Z:

$$R = \sum_{i=1}^{g} \left\{ P_i | \sum_{j=1}^{k} p_j^{(i)} \right\},$$
$$\sqrt{T} = \frac{\left|R^g \cap R^r\right| \left|Z_0 - Z\right|}{R^g \cup R^r}. \tag{4}$$

2.3. Magnetic Fluid Reynolds Equation of Oil Film Bearing. Reynolds' equation is the governing equation to study the film pressure produced by lubrication film in the process of lubrication. The general form is as follows:

$$\eta(x) = 2n\ln(L) + n\ln(h) + n\left\{\frac{n + tr(S)}{n - 2 - tr(S)}\right\} * DV, \tag{5}$$

$$U\left(d_i, w_j\right) = P(d_i)P\left(w_j|d_i\right); P\left(w_j|d_i\right) = \sum_{k=1}^{K} b\left(w_j|z_k\right)P\left(z_k|d_i\right), \tag{6}$$

where η indicates the viscosity of the lubricant, in PA s. U is the velocity of the upper surface in M/s. P is the hydrodynamic pressure in PA. H is the thickness of the oil film, in μ m. In a small area, the surface is simplified to a plane. Each texture unit is a square with length L, and there is a diamond texture with diagonal length B in it. The initial clearance of friction pair is H_0, the depth of microtexture is HP, and the oil film thickness between friction pairs can be expressed as follows:

$$L_i = IR * \beta\left(hp_i, v_i\right) + \sum_{j=1}^{p} \beta_j(x, y)x_{ij} + \varepsilon_j\beta_j, \tag{7}$$

where (x, y) denotes any point in the element. Δ indicates rhombic texture region. Dimensionless can reduce the number of variables in the process of solving, and also the solutions expressed by dimensionless parameters are universal. The dimensionless parameters are defined as follows, where P_0 is atmospheric pressure. By substituting the above equation into equations (6) and (7), the dimensionless Reynolds equation and film thickness equation can be obtained, respectively:

$$L\left(Y_i, y_i\right) = -\frac{1}{n}\sum_{i=1}^{n}\left[Y_i\log\left(y_i\right) + \left(1 - Y_i\right)\log\left(1 - y_i\right)\right], \tag{8}$$

$$p_0(\varepsilon) = \begin{cases} 0, & x_{ik}(\Lambda) = \dfrac{N}{A}, \quad x_{jl}(\varepsilon) = \dfrac{N}{A}; \\ 1, & x_{ik}(\Lambda) = Y_i\log\left(y_i\right) + \left(1 - Y_i\right)\log\left(1 - y_i\right), \quad x_{jl}(\varepsilon) = \dfrac{N}{A}, \end{cases} \tag{9}$$

where Λ indicates the operating condition of the friction pair. By substituting the above difference results into equation (9), the discrete form can be obtained as follows:

$$N(A) = K(y(T-1), \ldots, y(t-n), u(T-d-\phi), \ldots, u(k-d-n)),$$
$$Y(T) = K(y(k2-1), u(\rho 2 - c2 - 1)), \tag{10}$$

where ρ_2, C_2, and K_2 are the thermophysical parameters of MHD mixed with tumor tissue. φ represents the volume fraction of magnetic fluid in tumor tissue, and $\varphi = 003$ is the typical dose of the magnetic field. The thermophysical parameters of MHD are also replaced by the structure of MHD particles.

3. Preparation and Performance Test of Magnetic Fluid

3.1. Research Content. First of all, a device for simulating a microgravity environment with magnetic compensation is fabricated. The compensation device is an important part of the flat-topped long-pulse magnetic field device and is equivalent in the flat-topped phase of the magnetic field to a controlled current source to compensate for the magnet current. Its main functions are the fast and accurate acquisition of pulsed magnet currents, control of power devices (IGBT), fault handling, and human-machine interaction. The magnetic field generated by a pulsed magnet has a linear field; the magnetic field generated by the pulsed magnet has a linear relationship between field strength and current. Then, in the microgravity environment, according to the different proportions of magnetic solid particles, the base carrier liquid and the surfactant are mixed to produce nanomagnetic fluid, and the nanomagnetic fluid with different composition proportions is prepared by adjusting the proportion of ferrous and ferric ions. Finally, the lubrication performance of oil film-bearing magnetic fluid with different composition ratios was tested.

3.2. Preparation of Magnetic Fluid. In this paper, the nanomagnetic fluid used magnetic solid particles, base carrier liquid, and surfactant. Therefore, the focus of this study is to simulate the MHD lubrication model systematically, in order to make full use of the characteristics of MHD lubrication, such as good thermal uniformity, warm lubrication, adjustable parameters, and temperature control. In order to improve the reliability and safety of lubrication, the appropriate alternating magnetic field was designed, the accurate distribution of temperature field was obtained, the possible problems were discussed, and the treatment effect and safety were evaluated.

The lubrication coefficient includes thermal uniformity, temperature lubrication, active parameters, and temperature control. In the experiment, you can use the controlled variable method to implement one by one to find the specific relationship.

In order to prepare magnetic fluid, a TC4 bar was purchased and processed Φ 31.7 mm. For the blank sample with the size of 10 mm, the metallographic sandpaper with the particle size of 200, 400, 800, 1500, and 2000 was selected to polish the sample to RA < 0.2 μ m. We use an ultrasonic cleaning machine to clean for 10 min and air dry. The ylpd20 fiber laser was used to process the microtexture on the surface of the disk specimen. Through the preliminary setting test and continuous debugging, the laser output power was 6 W and the scanning speed was 100 mm/s. After laser processing, the workpiece is polished again with metallographic sandpaper, the material around the microtexture is cleaned, and the melted recast material is cleaned with acetone solution and dried.

Under certain conditions, the separated molecules or atoms are condensed, and the process of nucleation and growth of the condensate is controlled to obtain nanoparticle materials. Based on this principle, the metal carbonyl compound thermal decomposition method can prepare the ferromagnetic metal particle material S.8.0. Metal carbonyls are unstable and can be decomposed with changes in pressure and temperature. In the evaporator, the metal carbonyls vaporize and volatilize and are diluted by inert gas into the reaction vessel at a temperature of 25°C, and the metal carbonyls will decompose.

The preparation of the magnetic fluid base fluid uses ordinary kerosene, and the surfactant is selected as oleic acid. The whole process of the experiment is divided into dissolution, filtration, reaction, heating, separation, and other stages, and finally, a black shiny Fe304 kerosene-based magnetic fluid is obtained.

4. Results and Discussion

4.1. Magnetic Fluid Lubrication Performance. Figure 1 shows the relationship between the texture parameters and the coefficient of friction at temperatures of 30, 35, 38, 40, 43, and 50 degrees. Due to the extremely small size of the nanoparticles, when the friction subsurface is worn to form a crater, the nanoparticles gather at the dent to fill the wear in time, so that the friction subsurface is always in a flat state, by selecting the appropriate nanoparticles, so that the temperature-pressure reaction with the friction subsurface is firmly attached to the friction subsurface, so that the entire friction system has a self-healing function and thus has a friction reduction antiwear effect.

The effect of texture parameters on friction coefficient at different temperatures is shown in Figure 1. The lubricating fluid with a viscosity of 0.05 PAS was prepared by base carrier fluid and 9% NaCl. The surface motion parameters of the normal human hip joint were selected. The load was about 35 N, and the rotation speed was 83 R/min. The pressure sensor of the testing machine is 215b, the measuring range is 200 kg, and the sensitivity is 1.504 MV/v. The friction and wear tests were carried out in the form of a lubrication pool under simulated hydrodynamic lubrication for 30 min.

When the frequency is 100 kHz, the peak value of alternating current is 10 A, and the coil turns are 380, the distribution of magnetic field generated by Helmholtz coil is

shown in Figure 2. Electromagnetic exposure refers to the fact that the equipment of the information system can radiate through the ground wire, power line, etc. during operation, resulting in electromagnetic leakage. The magnetic field distribution refers to the distribution law of the magnetic field strength around the magnet. It can be seen that the magnetic field distribution near the magnetic fluid is more uniform; even if the patient's body moves forward and backward, left and right slightly, it can meet the requirements of magnetic fluid lubrication. It is worth noting that the magnetic field intensity decreases rapidly outside the coil device, and the electromagnetic exposure safety risk of patients' brains and nearby medical staff is low. The Helmholtz coil has a pair of identical current-carrying circular coils parallel to each other and coaxial, with current flowing in the same direction. Therefore, it is of great practical value in production and scientific research and is also commonly used as a measurement standard for weak magnetic fields.

The magnetic fluid is dense and sparse, and the electric field distribution is shown in Figure 3. The electric field intensity of the air in the magnetic fluid cavity is higher than that of the surrounding biological tissues, and the electric field intensity in the common bile duct outside the liver is about 190 V/m. The electric field intensity in the right hepatic duct is about 150 V/m, while that in the left hepatic duct is only 80 V/m. The location of one-dimensional magnetic field intensity distribution is along the direction of the common bile duct in the bearing magnetic fluid; that is, the magnetic field intensity at $x = 150$ mm is 9208 A/m. The uniformity of magnetic field distribution in space is the guarantee of safety and stability of MHD lubrication. Taking $x = 150$ mm as the center point, the variation range of magnetic field intensity in the range of 75 mm is not more than 0.3%. Compared with the single coil, the uniformity is greatly improved, and there is also a larger space suitable for lubrication.

Taking the magnetic field intensity $H = 9208$ A/m at the magnetic fluid as the external condition, the actual lubrication performance P of different attribute parameters of Fe_3O_4 magnetic medium under this condition is simulated and calculated by MATLAB. Magnetic fluid is a new kind of lubricant. It uses an external magnetic field to keep the magnetic fluid in the lubricated part without leakage. For example, mine wheel bearings are sometimes immersed in water, and water should be prevented from eroding the grease in the bearing and causing loss. Permanent magnets can be installed in the bearing to magnetize the rolling elements and form a magnetic field in the contact area between the rolling elements and the bearing ring. We keep the magnetic fluid lubricant in the bearing, so that the bearing is always in good lubrication conditions, thereby greatly improving the life of the bearing. The actual lubrication performance is related to the nanoparticle radius r, magnetic anisotropy parameter K, and viscosity coefficient of Fe_3O_4 magnetic fluid η and volume fraction φ as shown in Table 1. There are many kinds of magnetic fluids used in MHD lubrication, including ferrite magnetic nanoparticles Fe_3O_4 and Fe_3O_4. γ- Fe_2O_3 is a magnetic material approved by the US Food and Drug Administration and can be used in the human body. In this study, water-based Fe_3O_4 nanomagnetic fluid was used with a high Curie temperature of 120°C.

As shown in Figure 4, the actual lubrication performance is strongly dependent on the size of Fe_3O_4 nanoparticles and reaches the maximum value near $R = 9.5$ nm and then begins to decline. The reason is that when the radius of nanoparticles changes, the composite relaxation time also changes dynamically. When $r = 9.5$ nm, the Neill relaxation time is close to the brown relaxation time, and the composite relaxation time is the largest. When $R < 9.5$ nm, the relaxation is dominant, and the composite relaxation time and relaxation loss heat decrease. When $r > 9.5$ nm, the relaxation dominates, the equilibrium susceptibility decreases, and the actual lubrication performance decreases again.

As shown in Figure 5, in order to understand the lubrication of magnetic fluid under different lubrication performance in advance, this study carried out 8 times the simulation in advance; that is, when the actual lubrication performance of magnetic fluid is 5×105, 1×106, 1.5×106, and 2×106 w/m^3, the corresponding temperature data of MHD in hepatic hilum and MHD in the liver were obtained.

The lubrication time is 500 s, and the temperature of each point is summarized, as shown in Table 2. It can be seen that the temperature in the tumor is directly proportional to the actual lubrication performance of the magnetic fluid, the temperature in the center of the tumor is slightly higher than that in the edge, and the temperature in the corresponding point of the magnetic fluid model in the porta hepatis is slightly lower than that of the magnetic fluid model outside the liver. The optimal temperature range of MHD lubrication is 42~46°C. Therefore, as long as the minimum temperature of the tumor edge is above 42°C, it means that the magnetic fluid tissue can be effectively lubricated. According to the maximum temperature of 46°C, it can be preliminarily determined that when the actual lubrication performance of the magnetic fluid is at 1 and when the flow rate is about 106 w/m^3, it can meet the requirement of MHD lubrication.

The temperature required by the warm lubrication method and the simulation results of the Helmholtz coil is shown in Figure 6. Under the alternating magnetic field of 9208 A/M and 100 kHz, the calculated lubrication performance of the Fe_3O_4 magnetic nanoparticles is $P0 = 1.844 \times 106$ w/m^3 multiplied by the correction factor α. After the actual lubrication performance, $P = 1.014$. The SAR value of MHD is 4381.5 w/kg. The biological heat transfer module of COMSOL software was used to simulate the solution, and the free tetrahedral mesh was used to generate unit meshes. The research step was set as 1 s, and the total time was 500 s.

As shown in Figure 7, the magnetic anisotropy parameter is 1. The actual lubrication performance reaches the maximum at 104 J/m^3. The viscosity coefficient generally refers to the viscosity of the magnetic fluid-based carrier fluid. Nanomagnetic particles are dispersed in the base carrier fluid. Good fluidity enables them to enter the human tissue smoothly, and the viscosity coefficient is greater than 1. After 10 – 3 kg/(MS), the actual lubrication performance

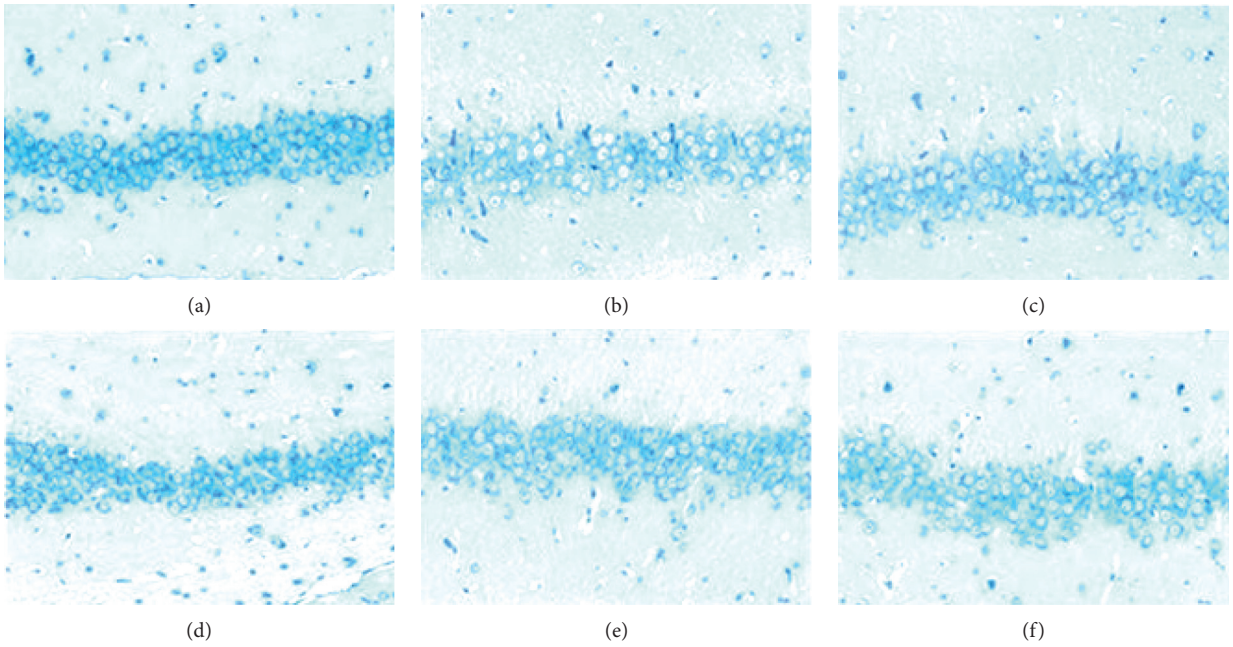

Figure 1: Influence of texture parameters on friction factor at different temperatures. (a) 30°C. (b) 35°C. (c) 38°C. (d) 40°C. (e) 43°C. (f) 50°C.

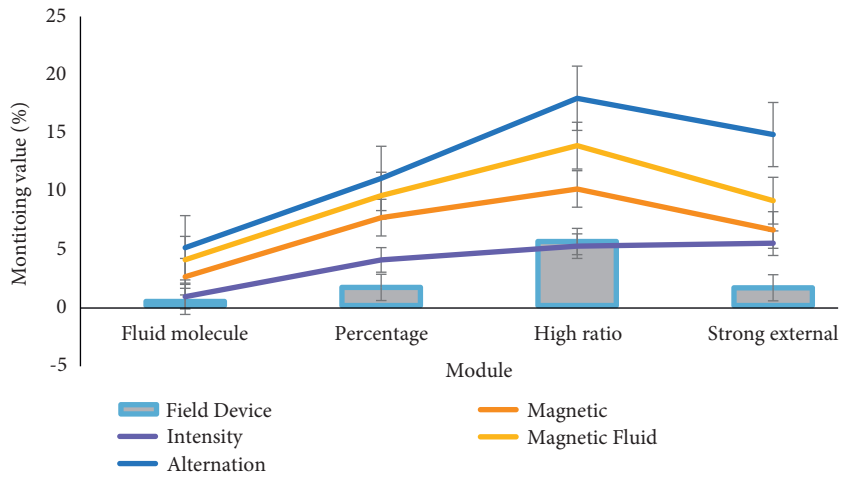

Figure 2: Distribution of the magnetic field generated by the Helmholtz coil.

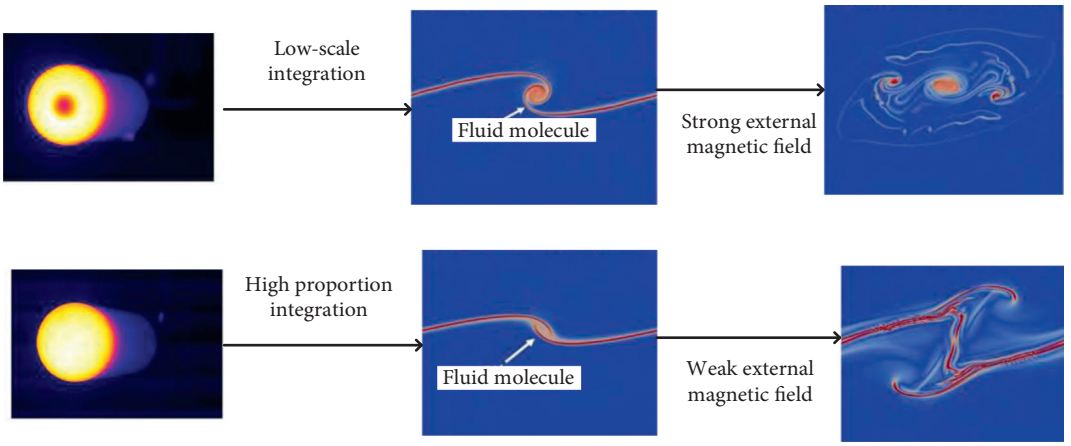

Figure 3: Magnetic fluid dense and sparse electric field distribution.

Table 1: The relationship between viscosity coefficient η and volume fraction φ.

Item	Intensity	Magnetic	Field device	Magnetic fluid	Alternation
P	0.76	1.71	0.35	1.45	1.04
φ	3.91	3.63	1.55	1.89	1.48
K	5.09	4.91	5.49	3.72	4.06
r	5.35	1.13	1.52	2.52	5.67
External	1.26	4.32	4.35	4.4	2.75

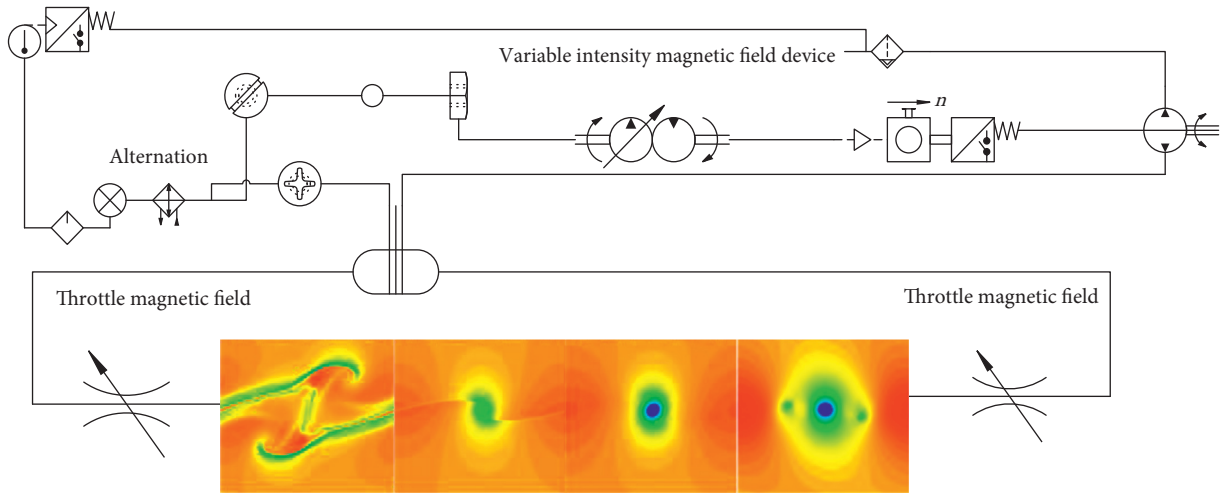

Figure 4: Dependence of actual heating power on nanoparticles.

tends to be stable. The actual lubrication performance is also in direct proportion to the volume fraction of the magnetic fluid. In a certain range, the lubrication degree of the tumor area can be increased or decreased by adjusting the volume fraction appropriately. The change of viscosity coefficient due to temperature change is not considered in this study.

The bearing deformation is evaluated by predicting the lubrication performance of small bearings, as shown in Table 3. Although the one-dimensional and two-dimensional bearing deformation models have high computational efficiency, the thermohydrodynamic lubrication model is extended to the thermoelastic hydrodynamic lubrication model when the size of the tilting pad journal bearing is large. Based on the model, a direct lubricated two-pad tilting pad journal bearing with a diameter of 890 mm is studied.

The results of the thermoelastic hydrodynamic lubrication model are shown in Figure 8. The static performance of tilting pad journal bearing under high speed and heavy load is studied and compared with the experimental results. A new 900 mm three-pad tilting pad journal bearing was optimized and verified. Through the coupling analysis of the thermal hydrodynamic lubrication program and commercial structural mechanics software, the influence of bearing thermal stress and deformation is considered. In this paper, the experimental study of a five-pad tilting pad journal bearing with directional lubrication is carried out under different oil supply flow conditions. By comparing with the theoretical results, it is found that speed has a great influence on the transition from rich oil to lean oil.

Table 4 shows the steady-state and dynamic performance of tilting pad journal bearing under the condition of too much lubricating oil and too low lubricating oil. The thermoelastic hydrodynamic lubrication models of tilting pad journal bearings are mostly solved by self-programming with finite difference method or finite element method. Because the programming code is not open source and not easy to copy, it limits the wide application of simulation tools in the industry. The great beauty of open source is that it is not dependent on a single vendor; everyone can modify the code to meet their own needs, and millions of "their needs" come together to make a great product. Using commercial software can make researchers pay more attention to physical phenomena than complex numerical methods. By combining COMSOL multiphysics and MATLAB, Hibachi's method is realized, which provides a new idea to solve the thermoelastic hydrodynamic model of coating cylinder line contact.

As shown in Table 5, under low preload, with the increase of excitation frequency, the dynamic contact lubricity of the solid-liquid interface keeps approximately unchanged, because the inherent properties (Poisson's ratio, elastic modulus) of the interface material remain unchanged, while the dynamic contact lubricity of the solid-liquid interface has an obvious increasing trend, and the variation laws of the two interfaces are consistent with the simulation results; however, the simulation results of the solid-liquid interface are slightly larger than the experimental data.

As shown in Figure 9, in the range of 80 Hz–100 Hz, the data value drops precipitously, which is inconsistent with the overall trend. It may be caused by the resonance between the excitation frequency and the experimental platform. Under high preload, with the increase of

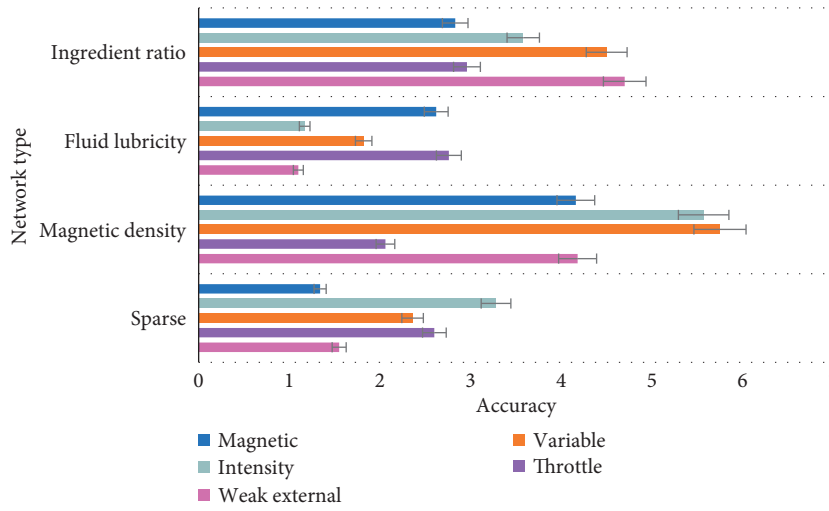

Figure 5: Lubrication of ferrofluid cancer.

Table 2: Lubrication time and temperature at each point.

Time (second)	Weak external	Throttle	Variable	Intensity	Magnetic
100	1.55	2.6	2.36	3.28	1.34
300	4.18	2.06	5.75	5.57	4.16
500	1.1	2.76	1.82	1.17	2.62
750	4.7	2.96	4.5	3.58	2.83

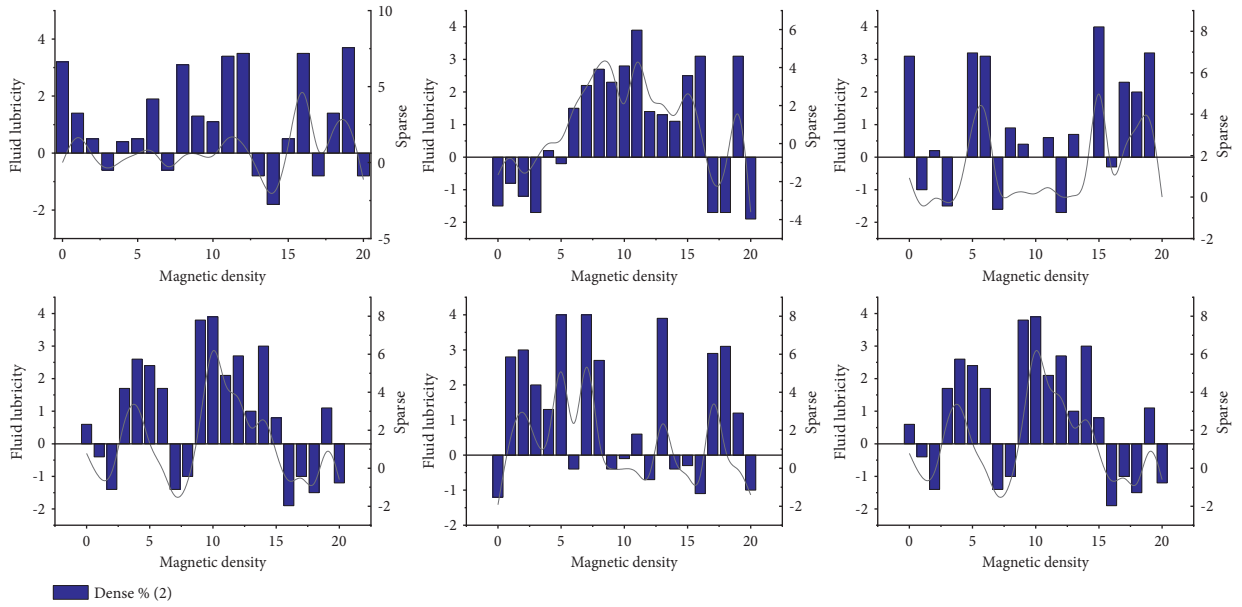

Figure 6: The relationship between ingredient ratio and lubricity.

excitation frequency, the change trend of solid-liquid interface and solid-consolidation interface is almost the same, but the solid-liquid interface still has a small increase, which is in good agreement with the theoretical model simulation. The differences in the range of 80 Hz–100 Hz are also caused by resonance.

As shown in Figure 10, when the ratio of Fe^{2+} to Fe^{3+} is between 11 : 20 and 13 : 20, the MHD lubrication performance of oil film bearing is in the peak region. When the ratio is 3 : 5, the best lubrication performance can be achieved. When it is slightly higher than this ratio, the oxidation rate is accelerated due to more ferrous ions. Although it can have a good lubrication effect, it is easy to cause the overall fluidity of oil film-bearing magnetic fluid to deteriorate. Therefore, the oil film-bearing nano-MHD with the ratio of 3 : 5 ferrous to ferric has the best lubrication performance in the microgravity environment simulated by magnetic compensation.

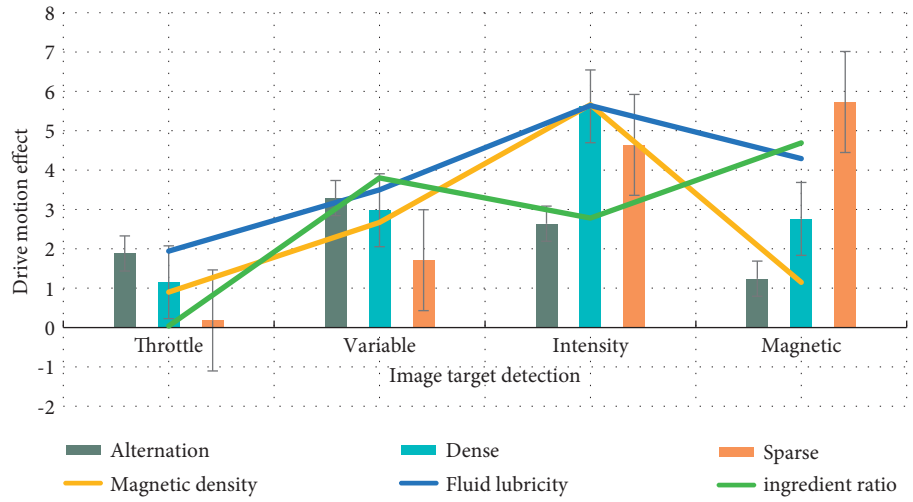

Figure 7: Volume fraction of magnetic fluid.

Table 3: Lubrication performance and bearing deformation of small bearings.

Item	Alternation	Dense	Sparse	Magnetic density	Fluid lubricity	Ingredient ratio
Throttle	1.88	1.15	0.18	0.9	1.94	0.04
Variable	3.29	2.98	1.71	2.67	3.5	3.8
Intensity	2.64	5.62	4.64	5.66	5.64	2.78
Magnetic	1.24	2.76	5.73	1.15	4.29	4.69

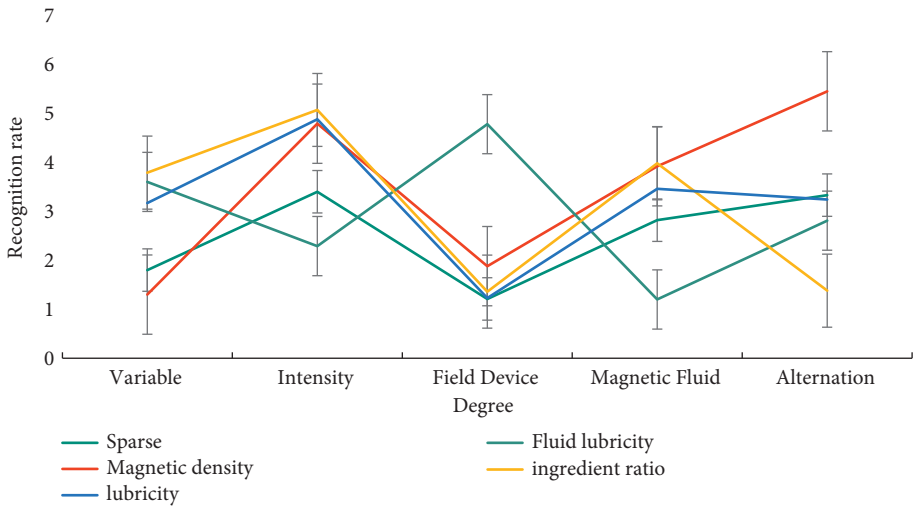

Figure 8: Thermoelastic hydrodynamic lubrication model results.

In the state of magnetic fluid lubrication, the amount of adhesive wear that occurs is the least. Different from the dry friction state and the traditional lubrication state, the surface is relatively smooth and smooth. The greater the load, the greater the amount of wear, and the maximum wear depth is 43.02 μm, 50.58 μm, and 150.1 μm, respectively. Under different load conditions, the wear depth of babbitt alloy under the magnetic fluid lubrication state is the smallest and the wear amount is the lowest. Under the traditional lubrication state, the friction and wear morphology has been improved, and the average friction coefficient is greatly reduced, mainly because the dry friction changes to wet friction and the lubricating oil plays a lubricating effect. In the state of magnetic fluid lubrication, the average friction coefficient is the lowest. The main reason may be that the nanomagnetic particles in the magnetic fluid fill the grooves and pits on the surface to play a certain role in repairing, and the nanoadditives in the magnetic fluid are in the process of wear. A series of physical and chemical reactions occur to form an oxide film on the friction surface, thereby effectively improving its friction and wear conditions.

Table 4: Steady state and dynamic performance of tilting pad sliding bearing.

Degree of occlusion	Sparse	Magnetic density	Fluid lubricity	Ingredient ratio	Lubricity
Variable	1.8	1.3	3.6	3.79	3.17
Intensity	3.4	4.79	2.29	5.07	4.88
Field device	1.21	1.88	4.78	1.36	1.23
Magnetic fluid	2.82	3.92	1.2	3.98	3.46
Alternation	3.33	5.45	2.81	1.38	3.24
Dense	4.11	4.26	4.39	6.73	1.73

Table 5: Approximate degree of dynamic contact lubricity of the joint surface.

Item	Alternation	Dense	Sparse	Magnetic density	Fluid lubricity
High ratio	3.83	1.14	3.66	3.39	1.21
External	2.41	5.84	2.82	3.17	2.31
Weak external	5.28	3.08	3.78	4.82	2.19
Throttle	2.3	2.43	4.06	3.64	1.15
Variable	4.62	1.22	6.34	6.71	6.25
Intensity	3.52	3.13	2.58	6.52	6.93

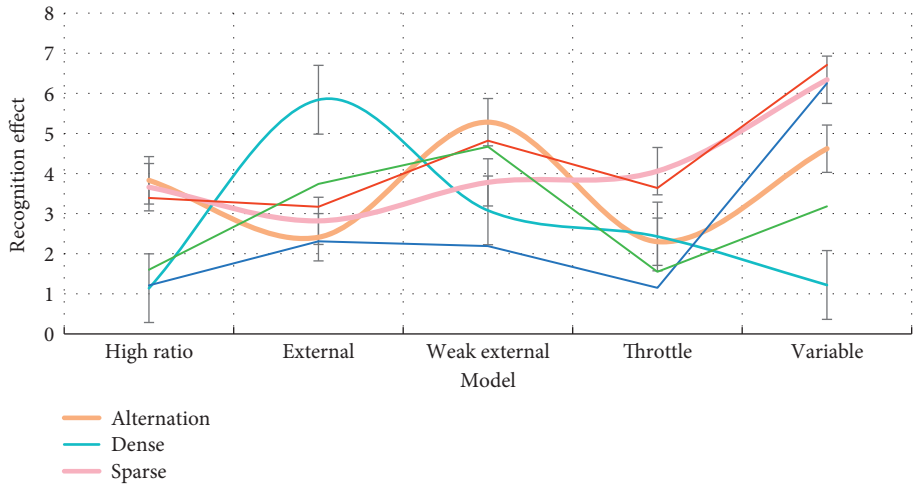

Figure 9: Excitation frequency and experimental platform resonance.

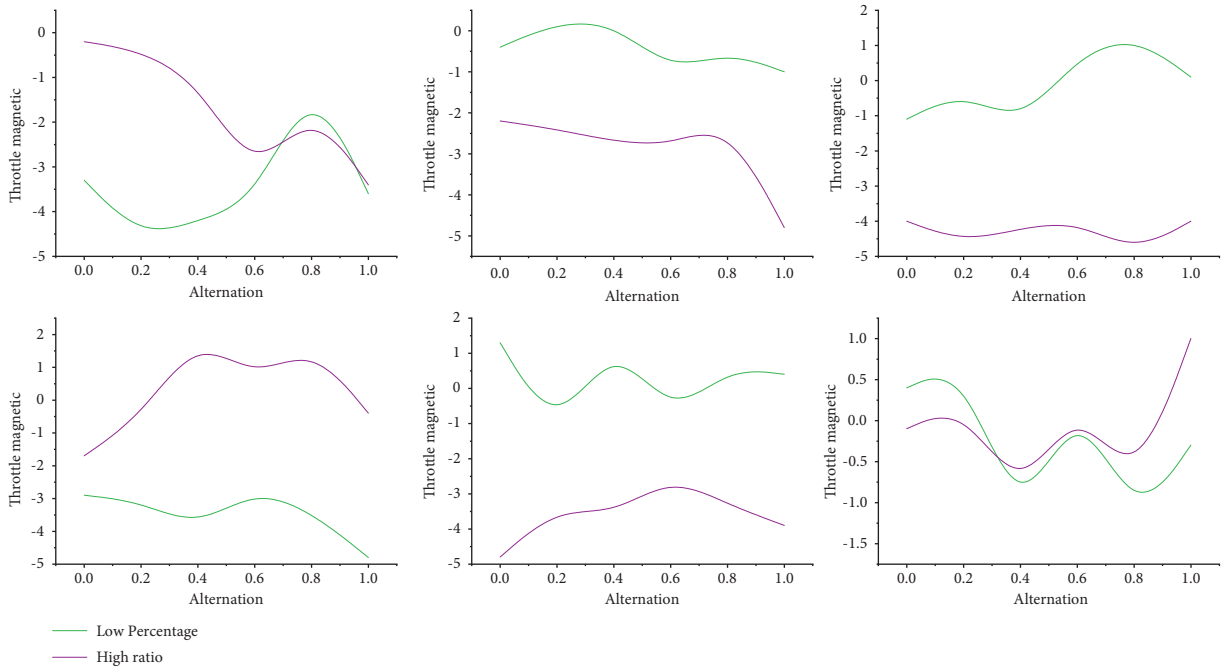

Figure 10: Influence of variable intensity magnetic field device on magnetic fluid.

4.2. Discussion. The purpose of this paper is to study the variation and relationship of oil film thickness, temperature distribution, pressure distribution, power loss, viscosity temperature characteristics, and leakage under constant temperature and variable temperature, vibration, and nonvibration conditions. Through the numerical simulation and friction and wear test, it can be concluded that the rhombic microtexture has the best parameters, which provides the basis for the subsequent optimization of texture parameters. The upper and right edges of the oil film bearing are closer to the magnetic field coil, so the magnetic fluid strength is higher. The temperature rise caused by the eddy current effect is more obvious here. In the vicinity of human skin tissue, the temperature increased by 4~5°C, and the temperature of other parts did not change significantly. In the process of changing with time, the temperature rises rapidly at the beginning and reaches the peak after about 10 minutes. It is worth noting that there is no obvious cumulative effect of heat during the long lubrication process of 30 min; that is, the temperature remains stable after reaching equilibrium and does not rise all the time. In the region of MHD lubrication, the temperature fluctuation caused by eddy heat is very small, which only increases by 0.1°C. Therefore, it can be considered that the eddy heat generated by the Helmholtz coil type magnetic field generator in this study will not cause harm to the human body under fixed parameters and has little influence on the temperature distribution in the tumor area of magnetic induction lubrication.

5. Conclusions

In this paper, the relationship between the parameters of Fe_3O_4 magnetic fluid and its lubrication performance is analyzed, and it is substituted into Pennes biological heat transfer equation as an external heat source term. Based on the finite element method, the model is meshed to obtain the distribution of electromagnetic field and thermal field in the MHD treatment area. When the frequency is 100 kHz, the peak value of alternating current is 10 A, the number of turns is 380, the amplitude of the magnetic field generated by the Helmholtz coil in MHD is 9208 A/m, and the distribution is relatively uniform. Based on the Reynolds equation, the hydrodynamic lubrication theoretical analysis model of biomimetic microtexture is established. The influence of texture size and texture depth on friction coefficient is solved by MATLAB. It is concluded that changing texture parameters can affect the friction performance of friction pairs, and the friction coefficient first increases and then decreases with the increase of microtexture size and depth. Under the condition of fluid lubrication, the experimental results are consistent with the numerical simulation results. By changing the parameters of microtexture, the friction behavior of the friction interface can be adjusted to achieve friction reduction. The different material properties, such as radius of nanoparticles, viscosity coefficient, magnetic anisotropy constant, and volume fraction, will lead to the change of the heating effect. It can meet the requirements of the warm lubrication method commonly used in MHD lubrication. There are also many shortcomings in this article. For example, due to the limitations of realistic conditions, this experiment was done hurriedly, and many details were not considered. This problem needs follow-up improvement.

Data Availability

No data were used to support this study.

Conflicts of Interest

The authors declare that there are no conflicts of interest.

Acknowledgments

This work was supported by Research on Magnetic Fluid Lubrication in Microgravity Environment (19-163-21-TS-001-028-01) and a Training Plan for Young Backbone Teachers of North China University of Water Resources and Hydropower in 2020.

References

[1] T. Kakutani, "Axially symmetric stagnation-point flow of an electricallyconducting fluid under transverse magnetic field," *Journal of thePhysical Society of Japan*, vol. 15, no. 4, pp. 688–695, 2020.

[2] M. F. Romig, "The influence of electric and magnetic fields on heattransfer to electrically conducting fluids," *Advances in Heat Transfer*, vol. 1, no. 4, pp. 267–354, 2020.

[3] R. W. Ziemer and W. B. Bush, "Magnetic field effects on bow shock stand-offdistance," *Physical Review Letters*, vol. 1, no. 2, pp. 58-59, 2020.

[4] D. R. Smith, D. E. Gildfind, P. A. Jacobs et al., "Magneto-hydrodynamic drag measurements in an expansion tunnel with argon test gas," *AIAA Journal*, vol. 58, no. 10, pp. 4495–4504, 2020.

[5] T. Murakami and Y. Okuno, "High-performance nonequilibrium-plasmamagnetohydrodynamic electrical power generator using slightlydivergent channel configuration: II. Experiment," *Journal of Physics D: Applied Physics*, vol. 41, no. 12, pp. 23–25, 2018.

[6] C. B. Su, Y. H. Li, and B. Q. Chen, "Experimental investigation of MHD flowcontrol for the oblique shock wave around the ramp in low-temperaturesupersonic flow," *Chinese Journal of Aeronautics*, vol. 22, no. 1, pp. 22–32, 2020.

[7] W. Zhao, Z. L. Jiang, T. Saito, J. M. Lin, H. R. Yu, and K. Takayama, "Performance of a detonation drivenshock tunnel," *Shock Waves*, vol. 14, no. 4, pp. 53–59, 2019.

[8] Z. Ahmad, S. Lv, Z. Tang, A. Shah, and X. Chen, "Methoxy poly (ethylene glycol)-block-poly (glutamic acid)-graft-6-(2-nitroimidazole) hexyl amine nanoparticles for potential hypoxia-responsive delivery of doxorubicin," *Journal of Biomaterials Science, Polymer Edition*, vol. 27, no. 1, pp. 40–54, 2016.

[9] A. Gülhan, B. Esser, U. Koch et al., "Experimental verification ofheat-flux mitigation by electromagnetic fields in partially-ionized-argonflows," *Journal of Spacecraft and Rockets*, vol. 46, no. 2, p. 274, Article ID 28338, 2019.

[10] D. R. Smith, D. E. Gildfind, D. J. Mee, C. M. James, and B. V. Allsop, "Magnetohydrodynamic dragforce

measurements in an expansion tunnel using a stress wave forcebalance," *Experiments in Fluids*, vol. 61, no. 8, pp. 11–15, 2020.

[11] L. Qiu, X. Han, T. Peng et al., "Design and experiments of a high fieldelectromagnetic forming system," *IEEE Transactions on Applied Superconductivity*, vol. 22, no. 3, pp. 37–39, 2019.

[12] R. H. Levy, "A simple MHD flow with hall effect," *AIAA Journal*, vol. 1, no. 3, p. 698, Article ID 69948, 2020.

[13] M. Kawamura, A. Matsuda, H. Katsurayama et al., "Experimental on dragenhancement for a blunt body with electrodynamic heat shield," *Journal of Spacecraft and Rockets*, vol. 46, no. 6, pp. 1171–1177, 2019.

[14] M. Kawamura, Y. Nagata, H. Katsurayama, H. Otsu, K. Yamada, and T. Abe, "Magnetoaerodynamicforce on a magnetized body in a partially ionized flow," *Journal ofSpacecraft and Rockets*, vol. 50, no. 2, pp. 347–351, 2019.

[15] B. Gao, N. Xu, and P. Xing, "Shock wave induced nanocrystallization during the high current pulsed electron beam process and its effect on mechanical properties," *Materials Letters*, vol. 237, no. 15, pp. 180–184, 2019.

[16] S. V. Bobashev, Y. P. Golovachev, G. A. Kurbatov et al., "Experimental andnumerical investigation into the supersonic flow of a weakly ionizedplasma around a dihedral angle: magnetohydrodynamic control of theflow pattern and heat fluxes toward the wall," *Technical Physics*, vol. 54, no. 1, pp. 33–41, 2019.

[17] X. Xianzhen, H. Yangdong, W. Lianying, and W. Xi, "Experimental and modeling of vapor–liquid equilibria for mixed electrolyte solution systems," *Journal of Chemical & Engineering Data*, vol. 61, no. 7, pp. 2311–2320, 2016.

[18] R. J. Nowak and M. C. Yuen, "Heat transfer to a hemispherical body in asupersonic argon plasma," *AIAA Journal*, vol. 11, no. 11, pp. 1463-1464, 2020.

[19] X. Xianzhen, H. Yangdong, W. Lianying, and C. Xia, "A new model in correlating and calculating the solid-liquid equilibrium of salt-water systems," *Chinese Journal of Chemical Engineering*, vol. 24, no. 8, pp. 1056–1064, 2016.

[20] L. E. Hooks and R. C. Lewis, "Simplified magnetoaerodynamic flow relationsfor axisymmetric blunt bodies," *AIAA Journal*, vol. 5, no. 4, pp. 644–650, 2020.

[21] M. D. Ladyzhenskii, "Hypersonic flow past a body inmagnetohydrodynamics," *Journal of Applied Mathematics andMechanics*, vol. 23, no. 6, pp. 1427–1443, 2020.

[22] P. S. Lykoudis, "The Newtonian approximation in magnetic hypersonicstagnation-point flow," *Journal of the Aerospace Sciences*, vol. 28, no. 7, pp. 541–546, 2020.

[23] R. W. Porter and A. B. Cambel, "Theoretical aspects of blunt bodymagnetoaerodynamics. NASA Report N-1-66, 196660 Poggie J, Gaitonde DV. Magnetic control of flow past a blunt body:Numerical validation and exploration," *Physics of Fluids*, vol. 14, no. 5, pp. 1720–3161, 2020.

[24] R. P. H. Berton, "Analytic model of a resistive magnetohydrodynamic shock without Hall effect," *Journal of Fluid Mechanics*, vol. 842, no. 4, pp. 273–322, 2018.

[25] M. Brio and C. C. Wu, "An upwind differencing scheme for the equations ofideal magnetohydrodynamics," *Journal of Computational Physics*, vol. 75, no. 2, pp. 400–422, 2020.

[26] G. C. Zha, Y. Shen, and B. Wang, "An improved low diffusion E-CUSP upwindscheme," *Computers & Fluids*, vol. 48, no. 1, pp. 214–220, 2019.

[27] D. G. Maciel and E. Sávio, "Magnetic field applied to thermochemicalnon-equilibrium reentry flows in 2D–five species," *International Journal of Computational Fluid Dynamics*, vol. 29, no. 6, pp. 376–399, 2019.

[28] X. Xu, Y. Hu, L. Wu, and S. Zhang, "Experimental and modeling of vapor-liquid equilibria for electrolyte solution systems," *Journal of Chemical & Engineering Data*, vol. 59, no. 11, pp. 3741–3748, 2014.

[29] B. Ju and D. C. Barnes, "The Effect of Nonzero B on the numericalsolution of the magnetohydrodynamic equations," *Journal of Computational Physics*, vol. 35, no. 3, pp. 426–430, 2020.